Measurement of Polarized Valence Quark Distribution Functions using Polarized Proton and Deuteron Targets

Tamar Didberidze

PhD Proposal

Physics Department

Idaho State University

Pocatello, ID

March 2, 2010

Abstract

Semi-inclusive deep inelastic scattering experiments using longitudinally polarized hydrogen ($^{15}NH_3$) and deuterium ($^{15}ND_3$) targets and a longitudinally polarized electron beam can be used to measure the ratio of the polarized valence quark distribution function to the unpolarized. Semi-inclusive scattering identifies an electron scattering experiment in which the scattered electron and one hadron are detected in the final state. I propose to analyze an electron scattering data set collected using the CEBAF Large Acceptance Spectrometer (CLAS) at the Thomas Jefferson National Laboratory. The incident electron energy ranged between 1.6 GeV to 5.7 GeV. The electrons impinged on either a polarized proton or deuteron target. This work focuses on a kinematic region where the struck quark carries at least 30% of the nucleons total momentum ($x_b > 0.3$). The leptons scatter mostly from valence quarks in this kinematic region, allowing contributions from sea quarks to be neglected. The Measurements are able to distinguish between the predictions made by the hyperfine perturbed constituent quark model (CQM) and perturbative Quantum Chromodynamics (pQCD).

Introduction

Incident electron scattering has been used for more than 40 years to measure the structure of a nucleon, a neutron or a proton. Early experiments at the Stanford Linear Accelerator Center (SLAC) showed that a nucleon was really composed of constituents called quarks. The constituent quark model's describes of a nucleon as a combination of three quarks. According to the quark model, two of the three quarks in a proton are labeled as having a flavor "up" and the remaining quark a flavor "down". The two up quarks have fractional charge $+\frac{2}{3}e$ while the down quark has a charge $-\frac{1}{2}e$. All quarks are spin $\frac{1}{2}$ particles. In the quark model each quark carries one third of the nucleon mass.

While elastic scattering measures the ground state properties of a nucleon, inelastic scattering experiments are used to probe a nucleon's excited states. The experiments at the SLAC used high energy electrons

scattered by nucleons. The mediator between the target nucleon and coulomb scattering of an electron is the virtual photon. The four-momentum, Q, of the virtual photon serves as a measure of the resolution of the scattering and may be formulated as:

$$d = \frac{\hbar c}{Q} = \frac{0.2 \text{ GeV} \cdot \text{ fm}}{Q}.$$

The electron scattering data taken during the SLAC experiments revealed a scaling behavior, which was later defined as Bjorken scaling. The inelastic cross section was anticipated to fall sharply with Q^2 like the elastic cross section. However, the observed limited dependence on Q^2 suggested that the nucleons constituents are pointlike. Independently, Richard Feynman introduced the quark parton model where the nucleons are constructed by the three point like constituents, called partons.

Shortly afterwards, it was discovered that partons and quarks are the same particles. In the QPM the mass of the quark is much smaller than in the naive quark model. In the parton model the inelastic electron nucleon interaction via the virtual photon is understood as an incoherent elastic scattering processes between the electron and the constituents of the target nucleon. "In other words, one assumes that a single interaction does not happen with the nucleon as a whole, but with exactly one of its constituents."[1] In addition, two categories of quarks were introduced, "sea" and "valence" quarks. The macroscopic properties of the particle is determined by its valence quarks. On the other hand, the so called sea quarks, virtual quarks and antiquarks, are constantly emitted and absorbed by the vacuum.

A new theory, called quantum chromodynamics(QCD), proposed the presence of neutral particles called gluons to bind quarks. Gluons are able to interact with each other and create virtual quark anti-quarks pairs. In 1979, evidence of gluons was discovered in a "three jet event" at PETRA [2].

The above described models predict several observable such as mass and lifetime for several baryon resonances. The constituent quark model predicts energy states of baryons, which represent the ground states with respect to the orbital motion of the quarks. In addition, the negative-parity baryon resonances, which are the spatial excitation of the quarks, are well classified by the constituent quark model. However, the masses of particular resonances, such as A(1405) and N(1440) have not been shown by the CQM. On the other hand, the N(1440) baryon resonance and others were reproduced by lattice QCD [3].

The understanding of the spin structure in the nucleon remains a major challenge for hadron physics. The parton model predicts that quarks carry about $(67 \pm 7)\%$ of the total nucleon spin [4]. Experiments performed at the European Organization for Nuclear Research(CERN) by the European Muon Collaboration(EMC) determined that only $(20 \pm 5)\%$ of the nucleon spin is carried by the quarks. Other experiments at CERN(spin muon collaboration(SMC)) and SLAC([5] E142 E143) also disagreed with the naive quark parton model. This reduction is explained due to contribution of negatively polarized sea quark at low momentum fraction x, which is not included in quark models. The complete picture of the nucleon spin can be obtained by taking into account the spin contributions from the gluons, the sea quarks, and their orbital momentum. The spin of the nucleon can be written as the sum of the following terms [5] :

$$\frac{1}{2} = \frac{1}{2}\Delta\Sigma + \Delta G + L_z$$

where $\Delta\Sigma$ is the spin contribution from the quarks, ΔG - from the gluons and L_z - the orbital angular momentum contribution from the partons(quarks).

1 Physics Motivation

In inclusive deep inelastic scattering only the electron is detected in the final state while in the case of semi inclusive deep inelatic scattering a hadron is detected in coincidence with the scattered electron. Both physics processes can be characterized by the differential cross section. The cross section is proportional to the detection rate. The differential cross section for the inclusive deep inelastic scattering can be written in terms of a lepton and a hadronic tensor [6] :

$$\frac{d^2\sigma}{dxdQ^2} \propto L_{\mu\nu}W^{\mu\nu}$$

where the leptonic tensor $L_{\mu\nu}$ describes the coupling between the scattering lepton and the virtual photon. The hadronic tensor $W^{\mu\nu}$ - the absorption of the virtual photon by the target nucleon. The hadronic tensor contains the information about the nucleon structure. It can be written in terms of structure functions using symmetry arguments and conservation laws. However, the information about the spin distribution inside the nucleon is contained in the asymmetric part of the hadronic tensor, which can be obtained by taking the difference of the cross sections with opposite spin states of the initial electron beam.

The double spin asymmetry can be defined as the difference between the cross section observed when the spin of the initial electron beam is antiparallel($\sigma_{1/2}$) to the target nucleon spin and parallel($\sigma_{3/2}$) divided by the sum [7] :

$$A_1 = \frac{\sigma_{1/2} - \sigma_{3/2}}{\sigma_{1/2} + \sigma_{3/2}}$$

where the cross section difference for polarized case is given by

$$\frac{d^2\sigma_{1/2} - d^2\sigma_{3/2}}{dxdQ^2} = \frac{8\pi\alpha^2}{Q^4}\frac{y}{E}[(E + E^{'}cos\theta)g_1(x, Q^2) - \frac{Q^2}{\nu}g_2(x, Q^2)]$$

where E and $E^{'}$ are the initial and final energy of the electron, θ - the electron scattering angle, α - the strong coupling constant, Q^2 - the four momentum transferred squared, x and y - bjorken scaling variables. g_1 and g_2 are polarized structure functions which contain information on the spin structure of the nucleon. Measurement of the double spin asymmetry and the ratio of the polarized valence down quark distribution function to the unpolarized can be used to distinguish between two descriptions of nucleon structure. pQCD and a hyperfine perturbed constituent quark model both predict that when the scaling variable (x_b) is unity, the proton and neutron double spin asymmetries are also unity. On the other hand, the well-studied SU(6) constituent quark model for $x_b = 1$ states that $A_p = 5/9$ and $A_n = 0$. Semi inclusive double spin asymmetry measurements using the CLAS detector in combination with polarized proton and deuteron targets can be used to distinguish between prediction of pQCD and the hyperfine perturbed CQM, unlike inclusive scattering were they have the same predictions [8] .

Deep inelastic scattering has provided a wealth of information about quarks and gluons in the nucleon. Inclusive deep inelastic lepton-nucleon scattering experiments were used to measure the spin structure of the nucleon. A nucleon's spin can be expressed as the sum of the quark spins, the quark orbital momentum, and the total angular momentum of the gluons. Inclusive DIS provides information about the total quark spin contribution to the nucleon and a limited amount of information for the polarization of the sum of quarks and antiquarks. The reason is that the scattering cross section is proportional to the square of the charge of the nucleon quark.

On the other hand, semi inclusive deep inelastic scattering experiments, where the hadrons in the final state are detected in coincidence with the scattered lepton, are sensitive to individual quark flavors and is referred as the flavor tagging. The flavor tagging method requires the knowledge of the probabilities $D_q^h(z, Q^2)$ - so called fragmentation functions, that a quark of flavor q will fragment into a type h hadron [9]. In addition, it is known that at high values of x_b the sea quarks(like $\bar{u}$(up antiquark)) do not have a major contribution in the nucleon.

The polarized quark distribution functions can be extracted from SIDIS measurements using the quark flavor tagging method and exclude assumptions used in inclusive DIS measurements. In SIDIS the double spin asymmetry can be expressed in terms of the cross sections of final state hadrons produced in the experiment [7] :

$$A_1^h = \frac{\sigma_{1/2}^h - \sigma_{3/2}^h}{\sigma_{1/2}^h + \sigma_{3/2}^h}$$

where $\sigma_{1/2}^h$ $(\sigma_{3/2}^h)$ represents the semi inclusive cross section of type h hadrons produced in the final state when the spin of the initial electron beam was antiparallel(parallel) to the target nucleon spin.

The semi-inclusive cross section can be expressed in terms of quark distribution functions and fragmentation functions:

$$\frac{d^3\sigma^h_{1/2(3/2)}}{dxdQ^2dz} \approx \Sigma_q e_q^2 q^{+(-)}(x,Q^2)D_q^h(z,Q^2)$$

The measured structure function in inclusive deep inelastic scattering experiments contains the contribution from all the different quark flavors to the total nucleon momentum and spin, without distinguishing the contribution from the individual quark flavors. Semi inclusive deep inelastic scattering experiments provide an opportunity to determine the struck quark flavor by detecting the hadron in the final state in coincidence with an electron.

The kinematics of single pion electroproduction in SIDIS can be described by five variables: the virtual photon four-momentum transferred squared Q^2, invariant mass of the photon-nucleon system W, the polar θ_π^* and the azimuthal angle φ_π^* of the outgoing pion in the center of mass frame and the scattered electron azimuthal angle φ_e.
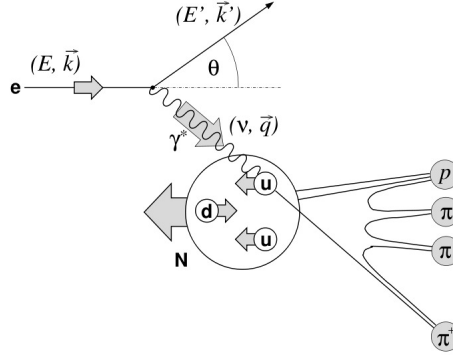

Figure 1. Diagram of The Semi Inclusive Deep Inelastic Scattering.

The incoming electron with four momentum $k = (E, \vec{k})$ is scattered from the target with four momentum $(M, \vec{0})$, where M represents the rest mass of the target nucleon. The four momentum of the scattered electron and hadron are respectively $k^{'} = (E^{'}, \vec{k'})$ and $p_h = (E_h, \vec{p_h})$. Semi inclusive deep inelastic scattering is depicted below on Figure. 1. The four momentum of the exchanged virtual photon, through which the SIDIS occurs, is the four momentum lost by the initial electron $q = k - k^{'}$. The negative square of the four momenta can be written as $Q^2 = -q^2|_{lab} = 4EE^{'}\sin^2\frac{\theta}{2}$, where Q^2 is greater then zero. The energy transferred from the scattering electron to the target nucleon, which is also the energy of the virtual photon, is given by

$$\nu = \frac{P \cdot q}{M} =^{lab} E - E^{'}$$

The Bjorken scaling variable x is defined as

$$x = \frac{Q^2}{2Pq} = \frac{Q^2}{2M\nu}$$

The energy fraction of the virtual photon transferred to a hadron, that is detected in the final state in coincidence with the scattered electron is

$$z = \frac{P \cdot p_h}{P \cdot q} =^{lab} \frac{E_h}{\nu}$$

where the last kinematical variable is the invariant mass of the scattering process available to produce the final hadronic state

$$W^2 = (q + P_h)^2 = M^2 + 2M\nu - Q^2$$

4

$k = (E, \vec{k}),\ k = (E^{'}, k^{'})$	4 - momenta of the initial and final state leptons
$\theta,\ \phi$	Polar and azimuthal angle of the scattered lepton
$P^{lab} = (M, \vec{0})$	4 - momentum of the initial target nucleon
$q = k - k^{'}$	4 - momentum of the virtual photon
$Q^2 = -q^2 \overset{lab}{=} 4EE^{'} \sin^2 \frac{\theta}{2}$	Negative squared 4 - momentum transfer
$\nu = \frac{Pq}{M} \overset{lab}{=} E - E^{'}$	Energy of the virtual photon
$x = \frac{Q^2}{2Pq} = \frac{Q^2}{2M\nu}$	Bjorken scaling variable
$y = \frac{Pq}{Pk} \overset{lab}{=} \frac{\nu}{E}$	Fractional energy of the virtual photon
$W^2 = (P+q)^2 = M^2 + 2M\nu - Q^2$	Squared invariant mass of the photon-nucleon system
$p_h = (E_h, \vec{p_h})$	4 - momentum of a hadron in the final state
$z = \frac{P \cdot p_h}{P \cdot q} \overset{lab}{=} \frac{E_h}{\nu}$	Fractional energy of the observed final state hadron

Table 1. Kinematic variables in deep inelastic scattering.

The electron scattering cross section off a nucleon can be written as [6] :

$$\frac{d^2\sigma}{dQ^2 dW^2} = \frac{2\pi\alpha^2 M}{(s - M^2)^2 Q^2}[2W_1(W^2, Q^2) + W_2(W^2, Q^2)(\frac{(s - M^2)(s - W^2 - Q^2)}{M^2 Q^2} - 1)]$$

and in the target rest frame it can be expressed in terms of the initial and final energies of electron and electron scattering angle θ:

$$\frac{d^2\sigma}{d\Omega dE^{'}} = \frac{\alpha^2 M}{8E^2 E_p \sin^4 \frac{\theta}{2}}[2W_1 \sin^2 \frac{\theta}{2} + W_2 \frac{4E_p^2}{M^2} \cos^2 \frac{\theta}{2}]$$

where W_1 and W_2 are so called structure functions, E_p and E the energy of the initial proton and electron respectively, θ - the polar angle of the scattered electron. M is the mass of the target, in our case the proton.

As it was mentioned above, the DIS interaction doesn't happen with the hadron as a whole, but with one of its constituents. Each quark(constituent) carries the fraction four-momentum x of the nucleon with probability density $q(x)$. $q(x)$ is the probability of finding the qth quark with fraction x of the nucleon four-momentum. Under these assumptions, the structure functions can be written as a sum of the elastic structure fractions weighted by $q(x)$. Taking into consideration that the mass of the ith quark is also the fraction x of the nucleon mass $M_q = xM_h$:

$$W_1(Q^2, \nu) = \Sigma_q \int_0^1 dx q(x) e_q^2 \frac{Q^2}{4x^2 M_h^2} \delta(\nu - \frac{Q^2}{2M_h x}) = \Sigma_q e_q^2 q(x_B) \frac{1}{2M_h}$$

and

$$W_2(Q^2, \nu) = \Sigma_q \int_0^1 dx q(x) e_q^2 \delta(\nu - \frac{Q^2}{2M_h x}) = \Sigma_q e_q^2 q(x_B) \frac{x_B}{\nu}.$$

The DIS of the unpolarized electron by a nucleon can be described in terms of two structure functions, $F_1(x)$ and $F_2(x)$ where:

$$F_1(x) = M_h W_1 = \frac{1}{2}\Sigma_q e_q^2 q(x)$$

and

$$F_2(x) = \nu W_2 = \frac{1}{2}\Sigma_q x e_q^2 q(x)$$

The relation between the structure functions $F_1(x)$ and $F_2(x)$ is given by the following equation:

$$F_2(x)\frac{1+\gamma^2}{1+R} = 2xF_1(x)$$

where $R(x,Q^2)$ is the ratio of longitudinal to transverse deep inelastic scattering cross sections and $\gamma = \sqrt{\frac{Q^2}{\nu^2}}$. In the naive quark parton model the longitudinal transverse interference is neglected. In the Bjorken limit it can be reduced to the Callan-Gross relation:

$$F_2(x) = 2xF_1(x)$$

The structure function F_1 measures the parton density, while F_2 describes the momentum density.

The distributions of up and down quarks in the nucleon are defined as u(x) and d(x). There are two categories of quarks: valence and sea quarks $u(x) = u_v(x) + u_s(x)$, assuming that $u_s(x) = \bar{u}(x)$. The constituent quark model (CQM or QPM) states that the proton(neutron) contains two up(down) quarks and one down(up) quark. Summing over all the constituents of a proton should result in the following sum rule:

$$\int_0^1 dx u_v(x) = 2$$

and

$$\int_0^1 dx d_v(x) = 1$$

The electromagnetic structure function for the proton and neutron can be expressed in terms of quark distribution functions:

$$F_2^{ep} = \frac{4}{9}[xu(x) + x\bar{u}(x) + xc(x) + x\bar{c}(x)] + \frac{1}{9}[xd(x) + x\bar{d}(x) + xs(x) + x\bar{s}(x)]$$

F_2^{en} can be obtained from F_2^{ep} by replacing u → d and vice versa. From the last two equations the structure functions for the proton and neutron can be written in terms of valence quark distribution functions:

$$F_2^{ep} = x[\frac{4}{9}u_v(x) + \frac{1}{9}d_v(x)]$$

and

$$F_2^{en} = x[\frac{4}{9}d_v(x) + \frac{1}{9}u_v(x)]$$

For most fixed-target experiments like EG1, the spin asymmetry is given by the ratio of the polarized structure function to the unpolarized: $A(x,Q^2) = \frac{g_1(x)}{F_1(x)}$, where the polarized structure function $g_1(x)$ represents the helicity difference of quark number densities. The spin asymmetry A and the unpolarized structure function F_1 are measurable quantities and through them one can determine $g_1(x)$, which maybe expressed as :

$$g_1(x) = \frac{1}{2}\Sigma_q e_q^2(q^+(x) - q^-(x)) \equiv \frac{1}{2}\Sigma_q e_q^2 \Delta q(x)$$

where $q^{+(-)}(x)$ is the quark distribution function with spin oriented parallel(antiparallel) to the spin of nucleon.

1.1 Fragmentation Independence

The asymmetries from semi inclusive pion electroproduction using proton or deuteron targets can be written in terms of the difference of the yield from oppositely charged pions [10] :

$$A_{1,p}^{\pi^+ \pm \pi^-} = \frac{\Delta\sigma_p^{\pi^+ \pm \pi^-}}{\sigma_p^{\pi^+ \pm \pi^-}}$$

$$A_{1,2H}^{\pi^+ \pm \pi^-} = \frac{\Delta\sigma_{2H}^{\pi^+ \pm \pi^-}}{\sigma_{2H}^{\pi^+ \pm \pi^-}}$$

Independent fragmentation identifies the process in which quarks fragment into the hadrons independent of the photon-quark scattering process, or in other words the fragmentation process is independent of the initial quark environment which starts the hadronisation process. Assuming independent fragmentation and using isospin and charge conjugation invariance for the fragmentation functions, the following equality holds:

$$D_u^{\pi^+ \pm \pi^-} = D_u^{\pi^+} \pm D_u^{\pi^-} = D_d^{\pi^+ \pm \pi^-}$$

The polarized and unpolarized cross sections for pion electroproduction can be written in terms of valence quark distribution functions in the valence region as:

$$\Delta\sigma_p^{\pi^+ \pm \pi^-} = \frac{1}{9}[4(\Delta u + \Delta\bar{u}) \pm (\Delta d + \Delta\bar{d})]D_u^{\pi^+ \pm \pi^-}$$

$$\Delta\sigma_n^{\pi^+ \pm \pi^-} = \frac{1}{9}[4(\Delta d + \Delta d^-) \pm (\Delta u + \Delta u^-)]D_u^{\pi^+ \pm \pi^-}$$

$$\Delta\sigma_{2H}^{\pi^+ \pm \pi^-} = \frac{5}{9}[(\Delta u + \Delta\bar{u}) \pm (\Delta d + \Delta\bar{d})]D_u^{\pi^+ \pm \pi^-}$$

and unpolarized:

$$\sigma_p^{\pi^+ \pm \pi^-} = \frac{1}{9}[4(u + \bar{u}) \pm (d + \bar{d})]D_u^{\pi^+ \pm \pi^-}$$

$$\sigma_n^{\pi^+ \pm \pi^-} = \frac{1}{9}[4(d + \bar{d}) \pm (u + \bar{u})]D_u^{\pi^+ \pm \pi^-}$$

$$\sigma_{2H}^{\pi^+ \pm \pi^-} = \frac{5}{9}[(u + \bar{u}) \pm (d + \bar{d})]D_u^{\pi^+ \pm \pi^-}$$

In the valence region ($x_B > 0.3$), where the sea quark contribution is minimized, the above asymmetries can be expressed in terms of polarized and unpolarized valence quark distributions:

$$A_{1,p}^{\pi^+ \pm \pi^-} = \frac{4\Delta u_v(x) \pm \Delta d_v(x)}{4u_v(x) \pm d_v(x)}$$

$$A_{1,2H}^{\pi^+ \pm \pi^-} = \frac{\Delta u_v(x) + \Delta d_v(x)}{u_v(x) + d_v(x)}$$

The ratio of polarized to unpolarized valence up and down quark distributions may then be written as

$$\frac{\Delta u_v}{u_v}(x, Q^2) = \frac{\Delta\sigma_p^{\pi^+ \pm \pi^-} + \Delta\sigma_{2H}^{\pi^+ \pm \pi^-}}{\sigma_p^{\pi^+ \pm \pi^-} + \sigma_{2H}^{\pi^+ \pm \pi^-}}(x, Q^2)$$

and

$$\frac{\Delta d_v}{d_v}(x, Q^2) = \frac{\Delta\sigma_p^{\pi^+ \pm \pi^-} - 4\Delta\sigma_{2H}^{\pi^+ \pm \pi^-}}{\sigma_p^{\pi^+ \pm \pi^-} - 4\sigma_{2H}^{\pi^+ \pm \pi^-}}(x, Q^2)$$

The ratio of polarized to unpolarized valence quark distribution functions can be extracted using the last two equations.

1.2 Independent Fragmentation Function Test

A test of independent fragmentation can be performed with polarized proton and neutron targets. The ratio of the difference of polarized to unpolarized cross sections for proton and neutron targets $\Delta R_{np}^{\pi^+ + \pi^-}$ can be written in terms of the structure functions:

$$\Delta R_{np}^{\pi^+ + \pi^-} = \frac{\Delta \sigma_p^{\pi^+ + \pi^-} - \Delta \sigma_n^{\pi^+ + \pi^-}}{\sigma_p^{\pi^+ + \pi^-} - \sigma_n^{\pi^+ + \pi^-}} =$$

$$= \frac{(\Delta u + \Delta \bar{u}) - (\Delta d + \Delta \bar{d})}{(u + \bar{u}) - (d + \bar{d})} (x, Q^2) =$$

$$= \frac{g_1^p - g_1^n}{F_1^p - F_1^n} (x, Q^2)$$

The last expression of the asymmetry $\Delta R_{np}^{\pi^+ + \pi^-}$ was obtained from the following equations:

$$g_1^p - g_1^n = \frac{1}{6} [(\Delta u + \Delta \bar{u}) - (\Delta d + \Delta \bar{d})]$$

and

$$F_1^p - F_1^n = \frac{1}{6} [(u + \bar{u}) - (d + \bar{d})]$$

Independent fragmentation holds if the ratio of the difference of polarized to unpolarized cross sections for proton and neutron targets $\Delta R_{np}^{\pi^+ + \pi^-}$ depends only on x and Q^2 of the quantities g_1 and F_1 measured in deep inelastic scattering and is independent of z.

2 Experimental Setup

The CEBAF large acceptance spectrometer (CLAS), located in Jefferson Lab's Hall B was used to measure the final state particles resulting from the scattering of a polarized electron by a polarized nucleon. The CLAS uses six superconducting coils to establish a toroidal magnetic field encircling the incident electron's momentum direction. A set of three drift chambers are positioned to determine the trajectories of particles which pass through the 6 gaps between the magnet coils. The first drift chamber, Region 1 (R1), is placed at the entrance to the magnetic coil. A second chamber, Region 2 (R2), is placed in the center of the coils. The final chamber, Region 3 (R3), measures charged particle leaving the toroidal field. A total of 18 drift chambers are available to reconstruct the trajectory of charged particles passing through the magnetic field. After the drift chamber system, the CLAS detector is equipped with a Cherenkov counter for separating electrons from pions and with scintillators to determine the Time of Flight of a charged particle. An electromagnetic calorimeter is placed at the exit of the detector to detect neutral particles and improve the detector's ability to distinguish between electrons and hadrons.

Five different targets were used during the EG1 experiment: $^{15}ND_3$, $^{15}NH_3$, C_{12}, liquid He-4 and frozen N_{15}. The last three targets were used to isolate the contributions of the proton and deuteron from the other nucleons present when using the first two targets.
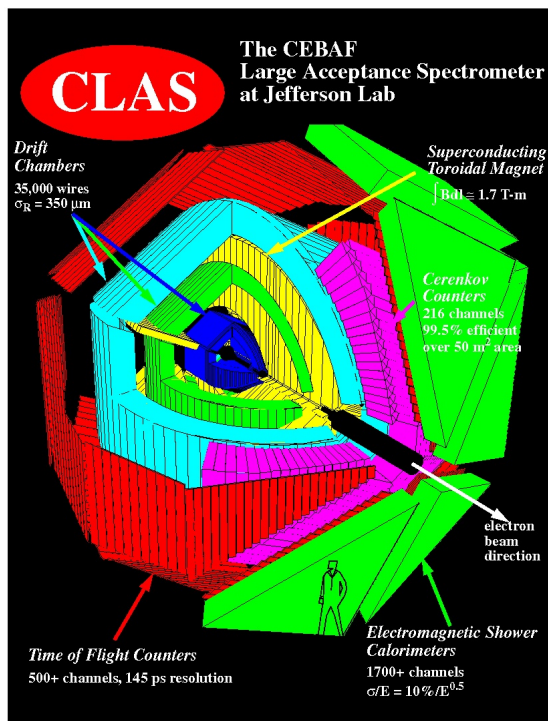
Figure 2. The CEBAF Large Acceptance Spectrometer at Jefferson Lab.

2.1 Target

2.1.1 Target Materials

The EG1 experiment at Jefferson Lab used five different targets to measure the polarized structure functions of the nucleon and perform background corrections [11]. The main target materials for the experiment used frozen ammonia, $^{15}NH_3$, for the polarized protons and deuterated ammonia, $^{15}ND_3$ for the polarized deuterons. A target ladder, placed 50 cm upstream of the standard CLAS target position, was used to position the desired target. The target ladder was designed and built in collaboration with the Italian Istituto di Fisica Nucleare, TJNAF, Oxford instruments and the University of Virginia. The solid targets NH3 and ND3 were polarized using the method of Dynamic Nuclear Polarization(DNP) achieving the average beam target polarization product for 5.7 GeV run $P_b \times P_t = (0.51 \pm 0.01)$ and $P_b \times P_t = (0.19 \pm 0.03)$ respectively [8] . Three other targets, C_{12}, liquid He_4 and solid N_{15} were used to remove the Nitrogen and Helium background from the NH_3 and ND_3 target data. Liquid Helium was used to cool the ammonia targets.

Dynamic Nuclear Polarization is a process in which the polarization of free electrons is transferred to a nucleus [12] . In DNP the target is doped with paramagnetic impurities by chemical doping or by irradiating the target in an electron beam. For low temperatures on the order of $0.5K$ and high magnetic fields on the order of 2.5Tesla, the free electron polarization approaches 100%, on the other hand the protons inside the target are unpolarized. An applied microwave field with a frequency close to the electron spin resonance induces transitions which flip the spin of the electron and nearby proton. The relaxation time of the electron is $10^{-3}s$, whereas the relaxation time of the proton in the target is 10^3s. Due to such a big difference of the relaxation time of the proton and electron, the flipped electron spin rapidly returns to its thermal equilibrium state from where it induces a proton spin-flip again. As a result, the spin polarization is transferred to the protons after some time.

Ammonia targets were selected because of their ability to produce high polarization and sensitivity to

electron high radiation dose by the incident electron beam radiation. The damage caused by this radiation can be repaired by annealing. The target is warmed up to liquid nitrogen temperature for annealing. In addition, the ammonia target has a high ratio of free nucleons (3/18) approximately 16.7 % for $^{15}NH_3$ and 28.6 % for $^{15}ND_3$. One disadvantage of choosing ammonia is the polarization background caused by ^{15}N(spin - 1/2), or ^{14}N(spin - 1), which was accounted for by taking data using a solid ^{15}N target [11] [13] .

2.1.2 Target Magnet

A 5 T magnetic field is established using a pair of superconducting Helmholtz coils oriented such that the magnetic field is parallel to the incident beam direction. The field induces the hyperfine splittings needed to polarize the target material using 140 Ghz RF waves. The uniformity of the field is varying less than 10^{-4} over a cylindrical volume of 20 mm in diameter and length. This configuration is necessary for DNP. The particles with scattering angles between 0-50 degrees are detected in the CLAS as well as 75-105 degrees. The Helmholtz coils block particles scattering between 50 and 75 degrees. The target magnetic field does not interact with the electron beam, however, it is effective in shielding the drift chambers from low energy Møller electrons. The target field bends the scattered particles in the azimuthal direction and falls rapidly with distance as ($1/r^3$). The effect of the magnetic field on the drift chambers is negligible [13] .

2.2 The CEBAF Large Acceptance spectrometer

2.2.1 The Torus Magnet

The CLAS's torus magnet consists of six superconducting coils located around the beam line in a toroidal geometry, producing a magnetic field in the φ direction when the z-axis of a spherical coordinate system is aligned with the incident beam direction. A sector is defined based on the boundaries of each magnetic coil resulting in a total of six sectors. The maximum current for the CLAS magnet is 2860 Amps corresponding to a total magnetic field in the forward direction of 2.5 T-m and 0.6 T at a polar scattering angle of 90 degrees. The magnet itself is around 5 m in diameter and 5 m in length. The coils of the magnet are cooled by liquid helium circulating through cooling tubes at the magnet's superconducting temperature of 4.5 K [14]. A charged particle's momentum is determined by the radius of curvature through the magnetic field to a resolution of $\Delta p/p$ from 0.5% to 1% [15]. In the EG1b experiment, the operated torus values were: 2250, -2250, 1500, -1500 Amps.

2.2.2 Drift Chambers

The drift chamber system in the CLAS detector is divided into three regions, each consisting of six separate chambers(sectors). The drift chambers contain three types of wires stretched between the endplates: sense, guard and field. The end plates are attached to the drift chamber so that the angle they form is equal to 60 degrees. Each drift chamber is subdivided into two separate superlayers. Each superlayer has six layers of drift cells. Each drift cell has one sense wire and is surrounded by six field wires forming a hexagonal shape. Each superlayer is surrounded by guard wires at a positive potential to complete the cell symmetry establishing a radial electric field within the drift cells. The sense wire is operated at positive potential and the field wire at negative. In each superlayer the distance between the sense and field wire increases with the radial distance from the target. In R1 the average distance between the sense and field is 0.7 cm, in R2 1.15 cm, and in R3 2.0 cm [16] . The CLAS drift chamber gas is a 90 - 10 % mixture of the argon(Ar) and CO_2, where Ar has an ionization gain of 10^4. Inside the drift chamber, a constant pressure is provided by outflowing the gas. The chamber end plates have circuit board with a single channel differential pre-amplifier for each sense wire.

The drift chamber system is used to track charged particles. A drift chamber is a particle tracking detector that measures the drift time of liberated electrons in a gas to calculate the spacial position of the ionizing particle. An electric field in a drift chamber is produced by the anode(sense) and cathode(field) wires. The charge particle traveling through the drift chamber ionizes the gas, freeing electrons that drift to the anodes. After a drift time (δt), electrons are collected at the anode(sense wire) generating a pulse for the

time measurement. The distance from the traversing particle to the known position of the sense wire can be calculated using the drift time and drift velocity.

2.2.3 Cherenkov detector

The threshold CLAS Cherenkov detector is used to distinguish electrons from pions. The gas mixture used to fill the Cherenkov counter is perfluorobutane C_4F_{10} gas at atmospheric pressure. The advantage of perfluorobutane C_4F_{10} gas is its high index of refraction n=1.00153, which results in a high photon yield. The threshold for Cerenkov radiation can be written as $v > c/n$, or for energies $E > \gamma \times m$, where v is the charged particle velocity, n the index of refraction for the medium, c the speed of light and $\gamma = \frac{1}{\sqrt{1-\frac{1}{n^2}}}$. In our case $\gamma = 18.098$. Accordingly, one can calculate the energy threshold for different charged particles; for electrons it is 9 MeV and for pions 2.5 GeV. The Cherenkov detector was designed to maximize the coverage in each of the sectors up to an angle $\theta = 45$ degrees [17] . Light is collected using a system of mirrors to focus the light onto cones which are connected to the Phillips XP4500B type photomultiplier tubes(PMTs). In the extreme regions of the spectrometer's angular acceptance, the number of detected photoelectrons is too low. To get acceptable efficiency in these regions, photomultiplier tubes were placed.

2.2.4 Scintillators

The CLAS is equipped with 288 scintillator counters. The scintillators are used to determine the time of flight for a charged particle and to determine coincidences between particles. The time of flight system has a time resolution at small polar angles of $\sigma = 120$ps and at angles above 90 degrees, $\sigma = 250$ps. This time resolution helps discriminate between pions and kaons up to 2 GeV/c. The time of flight system is located between the Cherenkov detectors and the electromagnetic calorimeters. The scintillator paddles, BC_408 [17], are located perpendicular to the average particle trajectory and have an angular polar coverage of 1.5 degrees. Each sector of the CLAS detector consists of 48 scintillator paddles with a thickness of 5.08 cm. The length of the scintillators varies from 30 cm to 450 cm and the width is between 15 cm at small polar angles and 22 cm for the large angles.

2.2.5 Calorimeter

The CLAS detector contains 8 electromagnetic calorimeter modules. A calorimeter is a device that measures the total energy deposited by a crossing particle. They are useful in detecting neutral particles and distinguishing between electrons and hadrons due to their different mechanisms of depositing energy. The CLAS calorimeter has three main functions: 1) detection of electrons at energies above 0.5 GeV; 2) detection of photons with energies higher than 0.2 GeV; 3) detection of neutrons, with discrimination between photon and neutrons using time-of-flight techniques. Calorimeter modules are placed in each sector in the forward region (polar angle of 10-45 degrees, forward angle calorimeter). Two modules are located at large angles in sectors 1 and 2(50-70 degrees, large angle calorimeter). The forward calorimeter has a lead/scintillator thickness ratio of 0.2, with 40 cm of scintillators and 8 cm of lead per module. The lead-scintillator sandwich is shaped to form an equilateral triangle in order to match the hexagonal geometry of the CLAS detector. Each scintillator layer contains 36 paddles parallel to one side of the triangle, with this configuration each orientation is rotated by 120 degrees from each other. This gives three views, each containing 13 layers providing stereo information locating the energy deposition. There is a longitudinal sampling of the shower to improve hadron identification. Each set of 13 layers were subdivided into 5 inner layers and 8 outer layers.

2.3 Experiment running conditions

Beam Energy	Torus Current	Begin Run	End Run	# trig(10^6)	expected # evts(10^6)	Target
5627	2250	27356	27364	56	19.4	12C
5627	-2250	27366	27380	130	13.6	15N
5627	2250	27386	27499	1210	20.2	NH3
5735	-2250	26874	27068	1709	19.9	12C
5735	2250	27069	27198	31509	15	MT
5764	-2250	26468	26722	1189	10	NH3
5764	-2250	26776	26851	662	15.9	NH3

Table 2. Experimental Running Conditions [18] .

3 Preliminary Results

The differential cross-section and asymmetries were measured using the CLAS with a 5.7 GeV continuous electron beam of $1.09209 \times 10^{33} \frac{[\# of electrons]}{second \times cm^2}$ luminosity when using the polarized targets above. A comparison was made with the results from experiment E99-107 [19] in order to benchmark the Ph.D. proposal's semi-inclusive analysis. Experiment E99-107 measured exclusive pion production using a liquid hydrogen target and the CLAS. The kinematics of single pion electroproduction can be described by five variables: the virtual photon negative four-momentum transfered squared (Q^2), invariant mass of the photon-nucleon system (W), the polar ($\theta_\pi{}^*$) and the azimuthal angle ($\varphi_\pi{}^*$) of the outgoing pion in center of mass frame and the scattered electron azimuthal angle (φ_e).
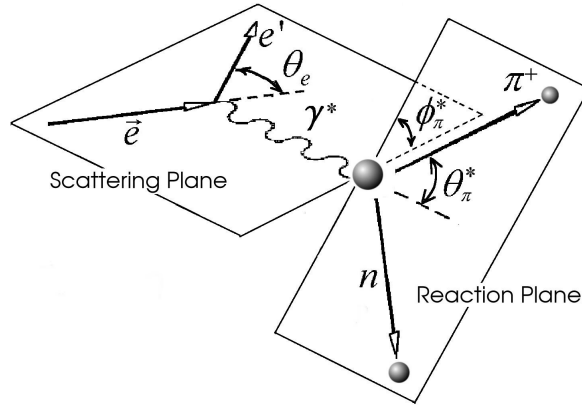

Figure 3. Kinematics of single π^+ electroproduction.

The five-fold differential cross section can be written in the following way for single pion electroproduction [19] :

$$\frac{\partial^5 \sigma}{\partial E_f \partial \Omega_e \partial \Omega_\pi{}^*} = \frac{1}{2\pi} \Sigma \frac{1}{L_{int} A_{cc} \epsilon_{CC} \Delta W \Delta Q^2 \Delta cos\theta_\pi{}^* \Delta \phi_\pi{}^*} \frac{d(W, Q^2)}{d(E_f, cos\theta_e)}$$

where L_{int} - the integrated luminosity, A_{cc} is the acceptance factor, ϵ_{CC} represents the efficiency of the cherenkov detector and the Jacobian term can be expressed in terms of the initial and final energy of lepton:

$$\frac{d(W, Q^2)}{d(E_f, cos\theta_e)} = \frac{2M_p E_i E_f}{W}$$

3.1 Cuts

The correct identification of an electron and a pion is the main requirement for a semi-inclusive analysis. Unfortunately, the pion is able to generate cerenkov radiation and as a result be misidentified as an electron. This contamination of the electron sample is removed using cuts on the energy deposited in the electromagnetic calorimeter, the number of photoelectrons in the Cherenkov counter, and fiducial cuts on the detector acceptance. The energy deposition in the calorimeter for electrons and pions is different. Pions are minimum ionizing charge particles. The energy deposited in the calorimeter by a pion becomes momentum independent once the pion momentum exceeds 0.08 GeV. On the other hand, electrons produce photoelectrons and generate an electromagnetic shower releasing the energy in the calorimeter which is proportional to their momentum. In order to remove contamination due to the energy deposition in the calorimeter the following cut was introduced: $EC_{total} > 0.2 * p$. A cut was also applied to the energy collected in the inner part of the calorimeter: $EC_{inner} > 0.06 * p$, because the ratio of the energy deposited in the total to the inner calorimeter depends on the thickness of the detector and is a constant.
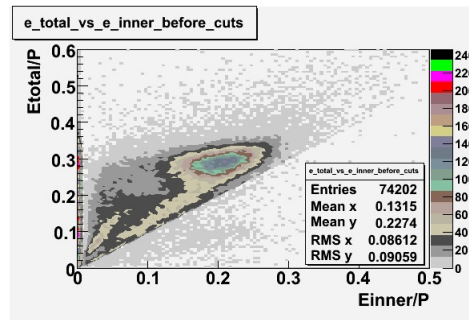

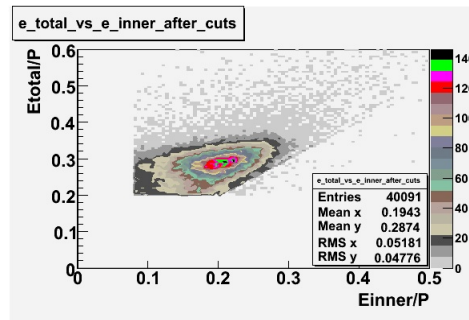Figure 4. E_{total} vs E_{inner} before cuts were applied.

Figure 5. E_{total} vs E_{inner} before cuts were applied.

In addition to the cut on the energy deposited into the electromagnetic calorimeter, the misidentified electrons were excluded by requiring a signal in the threshold CLAS Cherenkov detector. Pion's misidentified as electrons have been shown to produce around 1.5 photoelectons in the cherenkov detector, as shown in Fig. 6. Geometrical cuts on the location of the particle at the entrance to the cerenkov detector were applied to reduce the pion contamination. Fig. 7 shows that after cuts the peak around 1.5 is substantially reduced.
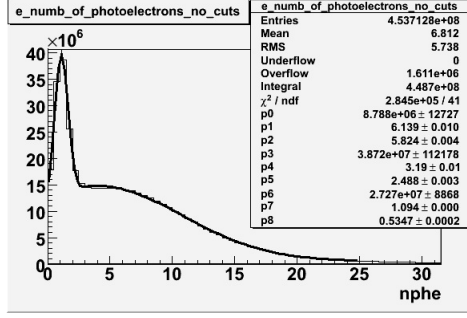
Figure 6. The number of photoelectrons without cuts.

The number of photoelectrons measured by the cherenkov detector is shown in Fig. 5. The number of pions which contaminate the electron candidate sample was estimated by fitting the photoelectron distribution with two Gaussian distributions and a Landau distribution. Integrals of the fits over the region of interest are used to determine the pion contamination to the electron candidates.

$$N_{pe} = p_0 e^{-0.5\left(\frac{x-p_1}{p_2}\right)^2} + p4\frac{1}{1 - \left(\frac{x-p5}{p6}\right)} + p_6 e^{-0.5\left(\frac{x-p_7}{p_8}\right)^2}$$

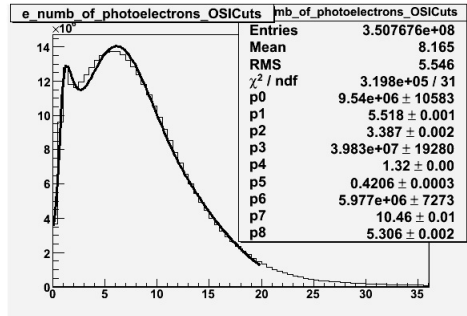| Distributions	Amplitude	Mean	Width
Gauss(0)	p0=8.788e+06 ±12717	p1=6.139 +0.01	p2=5.824 ±0.004
Landau(3)	p3=3.872e+07 ±112058	p4=3.19 ±0.01	p5=2.488 ±0.003
Gauss(6)	p6=2.727e+07 ±8869	p7=1.094 ±0.000	p8= 0.5347 ±0.0002

Table 3. Fitting Parameters with No Cuts.

Figure 7. The number of photoelectrons with OSI cuts.

Distributions	Amplitude	Mean	Width
Gauss(0)	p0=9.54e+06 ±10583	p1=5.518 ±0.001	p2=3.387 ±0.002
Landau(3)	p3=3.983e+07 ±19280	p4=1.32 ±0.00	p5=0.4206 ±0.0003
Gauss(6)	p6=5.977e+06 ±7273	p7=10.46 ±0.01	p8= 5.306 ±0.002

Table 3. Fitting Parameters with Cuts.

The pion contamination in the electron sample is $\sim 9.6\%$. In addition applying a cut on the number of photoelectrons, choosing events above 2.5 reduces the contamination to $\sim 4.03\%$.

Applying above described cuts and choosing events for the following kinematic region: $1.44 < W < 1.46$ and $0.4 < cos\theta_{pion}^{CM} < 0.6$ the pion polar angle in center of mass frame φ_π^* vs relative rate distribution is shown in Fig. 8 and compared with E99-107 data, which by itself is in agreement with the models.
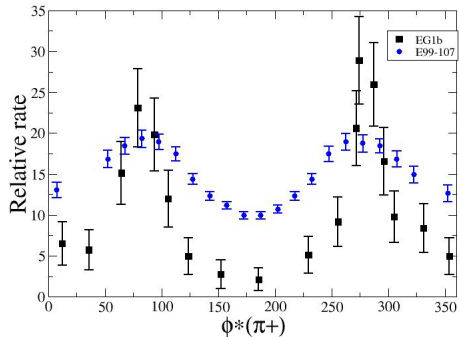
Figure 8. $\varphi_\pi{}^*$ vs Relative rate for fixed $cos\theta_{pion}^{CM} = 0.5$ and $W = 1.45 GeV$ [19] , [20] .

The EG1b data for kinematics chosen above shows the same shape as E99-107 data.
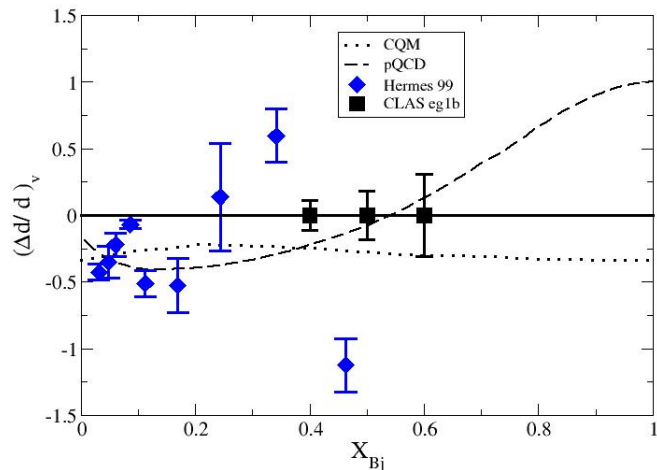

Figure 9. The ratio of polarized to unpolarized valence down quark distribution function vs x_{Bj} [21] .

In Fig. 9 the dashed line was achieved by fitting the world data with pQCD and the dotted line - by using a hyperfine constituent quark model wave functions. The diamond points represent HERMES collaboration results, with the statistical error bars. The solid square points represent the expected precision of this analysis.

4   Future Plans

The EG1 data shown in Fig. 8 was analyzed ignoring polarization by averaging over data with opposite polarization states. The next step in the analysis is to measure asymmetries using the knowledge of the probe and target's polarization state. These asymmetries are often referred as "double spin" asymmetries. Fig. 9 illustrates the three data points which are to be extracted by this analysis.

References

[1]   Dissertori, G., Knowles, I.K., & Schmelling, M. (2003). *Quantum Chromodynamics: High Energy Experiments and Theory*. Oxford, UK: Oxford University Press.

[2]   Brandelik, R., et al. (1979). Evidence for Planar Events in e^+ e^- Annihilations at High Energies. *Phys. Lett., B*(86), 243-249.

[3]   Arima, M., Masutani, K., & Sato, T. (2000). Baryon Resonances in a Constituent Quark Model. Progress of Theoretical Physics, Supplement, No. 137, 169-188.

[4]   Ellis, J., & Karliner, M. (1995). Determination of α_s and the Nucleon Spin Decomposition using Recent Polarized Structure Function Data. *Phys. Lett., B*(341)), 397-406.

[5]   Hommez, B. (2003). *A Study of Fragmentation Processes in the HERMES Experiments using a Ring Imaging Cherenkov Detector*. Doctoral dissertation. University of Gent (2003).

[6]   Roberts, R. G. (1990). *The structure of the proton. Cambridge Monographs on Mathematical Physics*. Cambridge, UK: Cambridge University Press.

[7]   Airapetian, A., et al. (The HERMES Collaboration). (2005). Quark helicity distributions in the nucleon for up, down, and strange quarks from semi-inclusive deep inelastic scattering. *Phys. Rev., D*(71), 012003.

[8]   Dharmawardane, K.V., et al., (The CLAS Collaboration). (2006). Measurement of the x and Q^2-Dependence of the Spin Asymmetry A1 on the Nucleon. *Phys. Lett., B*(641), 11.

[9]   Airapetian, A., et al. (The HERMES Collaboration). (2004). Flavor Decomposition of the Sea-Quark Helicity Distributions in the Nucleon from Semi-inclusive Deep inelastic scattering. *Phys. Rev. Lett.*, 92, 012005.

[10]   Christova, E., & Leader, E. (1999). Semi-inclusive production-tests for independent fragmentation and for polarized quark densities. hep-ph/9907265.

[11]   Keith, C. D., et al. (2003). A Polarized target for the CLAS detector. *NIM, A*(501), 327-339. 327-339.

[12]   Leader, E. (2001). *Spin in Particle Physics*. Cambridge, UK: Cambridge University Press.

[13]   Chen, S. (2006). *First Measurement of Deeply Virtual Compton Scattering with a Polarized Proton Target*. Doctoral dissertation. Florida State University, Tallahasee, FL.

[14]   Prok, Y. A. (2004). *Measurement of The Spin Structure Function $g_1(x, Q^2)$ of The Proton in The Resonance Region*. Doctoral dissertation. University of Virginia, Richmond, VA.

[15]   Fatemi, R. H. (2002). The Spin Structure of The Proton in The Resonance Region. Doctoral dissertation. University of Virginia, Sterling, VA.

[16]   Mestayer, M. D., et. al. (2000). The CLAS drift chamber system. NIM, A(449), 81-111.

[17]   Adams, G., Burkert, V. D., et al. (The CLAS Collaboration). (2001). The CLAS Cherenkov Detector. *NIM, A*(465), 414-427.

[18]   Fersch, R. (2007). Quality Checks. JLAB Hall-B Web site: http://www.jlab.org/Hall-B/secure/eg1/EG2000/fersch/QUALITY_CHECKS/file_quality/runinfo.txt.

[19]   Park, K., Burkert, V. D., & Kim, W. (The CLAS Collaboration). (2008). Cross sections and beam asymmetries for $\vec{e}$p $\rightarrow en\pi^+$ in the nucleon resonance region for $1.7 < Q^2 < 4.5$ $(GeV)^2$. *Phys. Rev., C*(77), 015208.

[20]   Burkert, V. D., & Minehart, R. (2005). E99-107 CLAS experiment. Measurement E14M16. CLAS database Web site: http://clasweb.jlab.org/cgi-bin/clasdb/msm.cgieid=14&mid=16&data=on.

[21]   Isgur, N. (1999). Valence Quark Spin Distribution Functions. *Phys. Rev. D*(59) 034013. hep-ph/9809255.